Appl Phys A (2011) 102: 877–883
DOI 10.1007/s00339-011-6270-y

Applied Physics A
Materials Science & Processing

Computational investigations into the operating window for memristive devices based on homogeneous ionic motion

Mohammad Noman · Wenkan Jiang · Paul A. Salvador · Marek Skowronski · James A. Bain

Received: 10 November 2010 / Accepted: 22 December 2010 / Published online: 19 January 2011
© Springer-Verlag 2011

Abstract A model that describes the homogeneous migration of oxygen vacancies as a function of electric field, temperature, and activation energy of diffusion was used to investigate the resistance switching and retention characteristics of memristive $SrTiO_3$ Schottky devices. Numerical simulations suggest that, though ionic motion results in switching, it is not possible to meet the criteria of fast switching and long retention simultaneously; conditions that lead to sufficiently fast switching also lead to unacceptably fast decays of programmed states. However, an operational window is found when a term accounting for local enhancement of electric field in the dielectric is included. A discussion of the appropriateness of this inclusion is provided.

1 Introduction

Over the last few years, there has been an increased interest in resistance-change random access memory (ReRAM), in which the memory cells (more recently named memristive devices [1]) are based on various oxide materials, such as $SrTiO_3$, TiO_2, NiO and others [2–5]. Owing to reported values of fast switching time, low current requirement, durability, scalability, and (potentially) long retention time, such devices are promising candidates for next generation memory technology [6, 7]. Several distinct mechanisms have been proposed to explain the switching behaviors, one of which is the homogeneous motion of donors, such as oxygen vacancies, within the oxide. For a specific class of devices, including the $SrTiO_3$ Schottky devices discussed herein, this donor motion has been identified as a main actor [8, 9]. Here we report on a computational investigation of donor motion in such devices to address the question: is a realistic operational window for data storage attainable?

Oxygen vacancies in oxides act as electron donors and are known to be mobile at room temperature [10]. It is possible to achieve a large redistribution of vacancies within the oxide under an electric field; and such redistribution can lead to resistance switching behavior [11]. The operation of various memory cells based on $SrTiO_3$ and TiO_2 has been explained qualitatively by this mechanism [3, 8, 9]. It is clear that a simple isothermal field-driven redistribution of vacancies, assuming field-independent mobility, will not result in dramatic distinction between switching and retention times [8]. Though several arguments have been proposed to overcome this issue, including field-dependent mobility coupled with thermal events during switching [12], the extent to which such effects can be applied to achieve the figures of merit required for data storage technologies is debatable.

To be competitive with existing memory technologies, memristive devices must switch in less than 100 ns and retain the programmed state for at least 10 years. If memories are to be designed using devices enabled by the uniform mo-

M. Noman (✉) · J.A. Bain
Department of Electrical and Computer Engineering, Carnegie Mellon University, 5000 Forbes Avenue, Pittsburgh 15213, USA
e-mail: mnoman@cmu.edu
Fax: +1-412-2683497

J.A. Bain
e-mail: jbain@cmu.edu

W. Jiang · P.A. Salvador · M. Skowronski
Department of Materials Science and Engineering, Carnegie Mellon University, 5000 Forbes Avenue, Pittsburgh 15213, USA

W. Jiang
e-mail: wenkan@cmu.edu

P.A. Salvador
e-mail: paulsalvador@cmu.edu

M. Skowronski
e-mail: mareks@cmu.edu

tion of oxygen vacancies, one must establish whether an appropriate range in timescales is obtainable. Here a physical model is presented that allows one to examine the dynamics of vacancy motion and to explore the interplay of various key governing parameters, such as temperature, applied and built-in electric fields, vacancy mobility, and its activation energy. It is important to note that the "uniform motion of vacancies" as used here applies to any system where the vacancy motion can be considered as 1-D where no lateral inhomogeneity of vacancy concentration or migration is significant. As such, along with completely homogeneous devices, this model is equally applicable to some forms of filamentary switching such as diffusion of vacancies along dislocation cores as proposed by Szot et al. [9]. More detailed discussion of the applicability of the model can be found in the Results and Discussion section.

2 Model

Here we focus on a model that describes a memristive device formed from a Schottky contact between an oxide having mobile donors and a high work function metal electrode such as Pt (which blocks ion transport). Several recent reports indicate that the effective Schottky barrier height can be modified by an external bias voltage that induces oxygen vacancy motion inside the oxide [3, 9, 13–15]. Since ionized vacancies are positively charged, their accumulation near the interface reduces the width of the Schottky barrier depletion region, whereas a depletion of vacancies has the opposite effect. This, in turn, modulates the tunneling current through the barrier, resulting in a resistance-change effect.

Following standard approaches to semiconductor simulation, the simultaneous solution of the Poisson equation (1) and continuity equations for electrons (2) and holes (3) was found computationally.

$$\nabla \cdot (-\varepsilon_r \varepsilon_o \nabla \psi) = q(p - n + N_D) \tag{1}$$

$$\frac{\partial n}{\partial t} = \frac{1}{q}\nabla \cdot (q\mu_n n\xi + qD_n \nabla n) \tag{2}$$

$$\frac{\partial p}{\partial t} = -\frac{1}{q}\nabla \cdot (q\mu_p p\xi - qD_p \nabla p) \tag{3}$$

In the above equations, ψ is the voltage, ε_r is the relative permittivity of the oxide, ε_o is the free space permittivity, q is the unit of electronic charge, p, n, and N_D are, respectively, the hole, electron, and ionized donor concentration, ξ is the electric field, $\mu_n(\mu_p)$ and $D_n(D_p)$ are the electron (hole) mobility and diffusion constant, respectively. For the electron (2) and hole (3) continuity equations, only the drift and diffusion currents were taken into account. Effects such as trap-assisted-tunneling or the thermal generation-recombination of carriers were ignored. All donors in (1) are considered to be singly ionized [16]. To account for the time dependence of the vacancy motion, (4) was used.

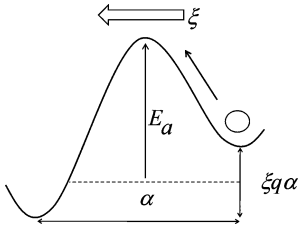

Fig. 1 Schematic of hopping model for vacancy migration. Electric field, ξ, changes the barrier height by $\xi q\alpha$ between the adjacent oxygen sites that are separated by a distance α. This gives rise to a non-linear dependence of the vacancy drift velocity on the electric field

$$\frac{\partial N_D}{\partial t} = -\frac{1}{q}\nabla \cdot J_{N_D} \tag{4}$$

In (4), J_{N_D} is the vacancy flux, which was modeled by a standard lattice-site hopping model, shown schematically in Fig. 1.

In Fig. 1, E_a is the activation energy barrier that exists for a vacancy to hop to an adjacent available lattice site in the crystal. However, an electric field can distort this barrier by $\pm\xi q\alpha$ on either side; where α is the jump distance. Using a Boltzmann distribution, we can write the expression for J_{N_D} considering the forward and backward hop rates.

$$J_{N_D} = \frac{1}{2}\alpha N_{D_L} f_o \exp\left(-\frac{E_a}{k_B T} + \frac{\xi q\alpha}{2k_B T}\right)\left(1 - \frac{N_{D_R}}{N_{D_{\max}}}\right) - \frac{1}{2}\alpha N_{D_R} f_o \exp\left(-\frac{E_a}{k_B T} - \frac{\xi q\alpha}{2k_B T}\right)\left(1 - \frac{N_{D_L}}{N_{D_{\max}}}\right) \tag{5}$$

Here, N_{D_L} and N_{D_R} represent the vacancy concentration on the left (6) and right side (7) of the energy barrier, respectively; k_B is the Boltzmann's constant and T is temperature. The maximum attainable vacancy concentration, $N_{D_{\max}}$, is related to the maximum oxygen site concentration in the crystal that can accommodate vacancies (thermodynamic factors were not included; which would explicitly describe the accommodation of defects as a function of the defect chemical potential within the crystal [17]).

$$N_{D_L} = N_D - \frac{\alpha}{2}\frac{dN_D}{dx} \tag{6}$$

$$N_{D_R} = N_D + \frac{\alpha}{2}\frac{dN_D}{dx} \tag{7}$$

The diffusion coefficient, D_o, is described by (8).

$$D_o = \frac{1}{2}\alpha^2 f_o \exp\left(-\frac{E_a}{k_B T}\right) \tag{8}$$

By substituting (6)–(8) into (5) and removing second order terms, a simplified form of (5) can be expressed as (9).

$$J_{N_D} = \frac{2}{\alpha} D_o N_D \sinh\left(\frac{\xi q \alpha}{2k_B T}\right)\left[1 - \frac{N_D}{N_{D_{\max}}}\right] - D_o \frac{dN_D}{dx} \cosh\left(\frac{\xi q \alpha}{2k_B T}\right) \quad (9)$$

When $\frac{\xi q \alpha}{2k_B T} \leq 0.1$ and $N_D \ll N_{D_{\max}}$, (9) reduces to the familiar Nernst–Einstein relationship. The 'drift' velocity of vacancies is defined from the first term of (9), and is given as

$$v_{N_D} = \frac{2}{\alpha} D_o \sinh\left(\frac{\xi q \alpha}{2k_B T}\right)\left[1 - \frac{N_D}{N_{D_{\max}}}\right] \quad (10)$$

Equations (1)–(4) (after substituting the expression for J_{N_D} from (9) into (4)) fully describe the model that we used to explore the transient characteristics of our memristive Schottky device. The transient characteristic of vacancy transport, as represented by (4) and (9), is coupled to the Schottky interface through the N_D term in (1). Any change in vacancy concentration affects the potential profile ψ of the device, which in turn affects the device current–voltage characteristics. Current flow through the device consists of the drift and diffusion components in (2) and (3), which captures the thermionic emission of carriers over the Schottky barrier. Additionally, a parallel channel of tunneling current is calculated in the vicinity of the Schottky interface following the scheme outlined in [21]. The parameters of most interest are ξ, T, and E_a, which control the timescale of switching and retention. We used (10) to calculate the drift velocity of vacancies that corresponds to specific switching and retention conditions.

3 Simulations

The above model was implemented on a 1-D Metal (M1)–$SrTiO_3$–Metal (M2) structure, as shown in inset of Fig. 2. M1 was modeled as a deep work function metal (5.8 eV), such as Pt, that forms a Schottky contact with vacancy-doped $SrTiO_3$, due to the work function mismatch between the two layers; and it was treated as a blocking interface, such that donors cannot cross the interface. M2 was modeled as a highly conductive oxide contact that forms an ohmic (work function of 4.25 eV), non-oxygen-blocking contact with $SrTiO_3$ (such as conductive $SrTiO_3$ or $SrRuO_3$ [13]). Therefore, M2 acts as a source or a sink of oxygen vacancies to the $SrTiO_3$ layer, as necessary. The vacancy concentration at the $SrTiO_3$/M2 interface was fixed at 1×10^{18} cm^{-3} throughout the simulation. The temperature was maintained at 300 K for all simulations (temperature effects can be discussed to first order by considering different ratios of E_a/T and ξ/T).

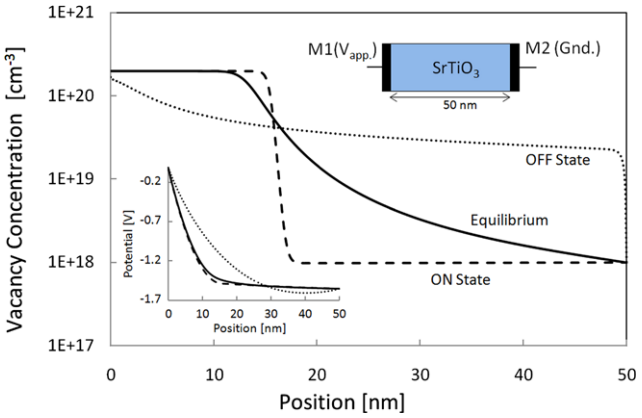

Fig. 2 Simulated plot of vacancy profile after application of ±5 V 100 ns programming pulses. The 'OFF' ('ON') state corresponds to a situation when tunneling current is reduced (increased). Vacancy activation energy is set to 0.2 eV. *Lower inset* shows corresponding potential profiles and *upper inset* shows the device structure

In all simulations, the thickness of the $SrTiO_3$ layer was set at 50 nm, similar to that expected in memory technologies. The bandgap of $SrTiO_3$ was taken to be 3.2 eV, the electron affinity to be 4.1 eV [18], and the mobility of electrons and holes to be 6 cm^2/V s and 5 cm^2/V s, respectively [19]. Initially, the doping was assumed to be uniform with a concentration of 1×10^{18} cm^{-3}. The reported value of activation energy for vacancy motion in $SrTiO_3$ varies between 0.6–2.2 eV [10, 20]. Instead of selecting a single specific value, we examined the ON/OFF dynamics as a function of the activation energy and electric field strength.

The four coupled differential equations (1)–(4) were solved iteratively. In this process, time stepping was carried out for (4), while the time-dependent portions of (2) and (3) were set to zero. This is reasonable because the mobilities of electrons and holes are much higher than the mobility of oxygen vacancies. Therefore, the electrons and holes achieve steady-state distributions instantaneously, when compared to the time scale of vacancy motion. The potential profile obtained from the self-consistent solution to (1)–(4) was used to calculate the tunneling probability through the Schottky barrier and the total tunneling current following the scheme described above. Total current through the device is the sum of this tunneling current, the drift ($q\mu_n n\xi$ & $q\mu_n p\xi$) and the diffusion ($qD_n\nabla n$ & $qD_n\nabla p$) currents obtained from (2) and (3). All voltage values reported are referenced to the M1 contact, while the M2 contact was assumed to be grounded.

4 Results and discussion

The presence of a large built-in electric field, owing to the small thickness of the $SrTiO_3$ layer and large work function difference between the two metal contacts (1.55 eV), acts

to modify the initial uniform vacancy concentration. The device was first equilibrated by determining the long-time solution to (1)–(4) using the initial configuration and zero applied external bias. The equilibrium profile is shown in Fig. 2 as the dark solid curve, for a low activation energy of 0.2 eV. Due to the built-in electric field, vacancies accumulate next to the Schottky contact. The maximum concentration allowed was 2×10^{20} cm^{-3} (9). The potential profile for this configuration is given in the inset of Fig. 2. As a result of injected vacancies from the M2 contact, the equilibrium Schottky barrier depletion width is much thinner than what would be expected for a uniform 1×10^{18} cm^{-3} initial vacancy concentration.

Once the equilibrium profile was achieved, a ± 5 V pulse was applied for 100 ns to program the device to either an ON or OFF state. As observed in Fig. 2 (the long dashed curves), the application of -5 V (ON) pulse causes the vacancy accumulation at the Schottky interface to increase, and thereby the tunneling current increases slightly. The potential profile is only modestly affected by this redistribution (inset of Fig. 2). The application of $+5$ V (OFF) 100 ns pulse has an opposite effect (dotted curve). The donors near the M1/$SrTiO_3$ interface region are largely depleted from the equilibrated values and are spread throughout the $SrTiO_3$ layer. This redistribution (there is little transfer of donors to the M2 contact) considerably affects the potential profile throughout the device (seen again in the inset of Fig. 2).

However, the profiles achieved immediately after the application of programming pulses are not stable. Given enough time, drift due to built-in electric field and diffusion due to concentration gradients will cause the vacancy distributions to be restored to the equilibrated profile. This effect, in essence, defines the retention characteristics of the device. Retention was investigated by determining the evolution of vacancy profiles as a function of time, in the absence of an applied voltage and using different values of the activation energy for vacancy hopping. In each case, the ON and OFF state vacancy profiles shown in Fig. 2 were used as the starting points (for the higher activation energies, these profiles are achievable, though they require longer than 100 ns to produce).

The current flowing through the device (e.g., at -1 V) was determined between time steps during the decay process; which is shown in Fig. 3 for activation energies of 0.2, 0.6, and 1.02 eV. It is clear that both states eventually merge to the same value, as expected, with higher activation energies taking longer. The initial changes in current with time are nearly linear on the log–log plot. However, the rate of change accelerates appreciably near the end (the OFF state has a complicated state of current owing to the profile evolution). Linear extrapolation of the early time data greatly overestimates the retention time of the devices.

If one defines the retention time of such devices as the time at which point the difference in current between the OFF and ON state is lower than two orders of magnitude, then the upper (lower) horizontal dash-dot line indicate the retention current for the ON (OFF) state. For an activation energy of 1.02 eV, this time is ≈10 years. For lower values of energies, the time is reduced drastically, ≈6.8 μs for 0.2 eV and ≈36 seconds for 0.6 eV. Essentially, a 1 eV hopping energy barrier allows for reasonable retention times. While these values correspond to $T = 300$ K case, retention characteristics under higher operating temperatures can be approximated from these results. Temperature dependence of vacancy flux mostly depend on the E_a/k_BT term in (9) (embedded in the D_o term) when the electric field is small (as is the case here with no external bias applied, such that the electric field dependence of vacancy mobility can be safely ignored). As an example, the 0.2, 0.6 and 1.02 eV curves in Fig. 3 would effectively correspond to 0.24, 0.72 and 1.22 eV, respectively, if the operating temperature of the device was 85°C rather than room temperature.

The initial profiles used to generate the retention curves in Fig. 3 resulted from the application of a 0.1 μs long ± 5 V pulse to a material with an activation energy of 0.2 eV, whose specific retention time was ≈6.8 μs. In other words, the retention time was only two orders of magnitude larger than the programming time. Similar results were observed for other activation energies, meaning the writing times to generate similar profiles to those shown in Fig. 3 are also only 1–2 orders of magnitude lower than the retention time, values unacceptable for data storage. Ideally, we would like to switch under the condition where the material behaved as if the activation energy for writing was ≈0.2 eV (at room temperature) and for reading was ≈1.02 eV. Three primary factors that control the timescale of programming are activation energy, temperature, and electric field. Just considering

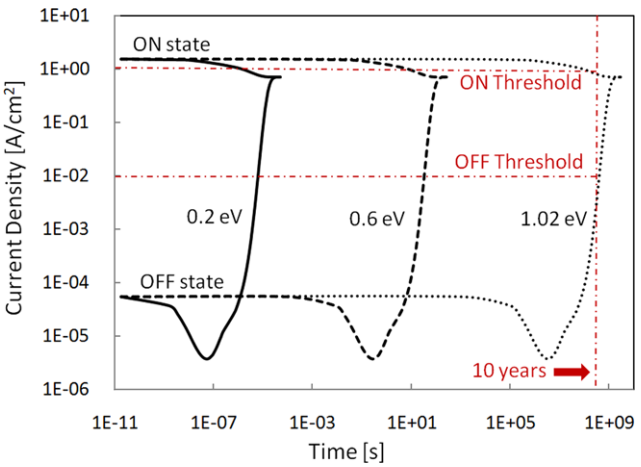

Fig. 3 Simulated current density measured at -1 V as a function of time for three different activation energies for vacancy migration. Current is measured periodically as the vacancy profile evolves from the programmed to equilibrium state. To achieve 10 years of retention, an activation energy of 1.02 or larger is necessary

temperature at the moment, a factor of 5 difference in the temperature during reading (300 K) and writing (1500 K) would lead to 10 year retention and 100 ns switching, but 1500 K is likely to be too high in realistic device.

To investigate the effects of the activation energy, temperature, and electric field on device characteristics, simulations were carried out for a range of those parameters. The simple question was: can one find a situation where the writing time is 100 ns and the retention time is ≈10 years? Based on the programming conditions used to generate the data in Fig. 2, using (10), we calculate a drift velocity of 0.67 nm/ns. This velocity leads to a programming time under 100 ns (for this specific state). Similarly, using the 1.02 eV situation described for the data presented in Fig. 3, the drift velocity is found to be 3.3×10^{-15} nm/ns, which results in 10 year retention. The drift velocity was extracted using the applied (built-in) field of 1 (0.31) MV/cm for programming (retention).

By carrying out a similar procedure for a range of parameters, we determined the drift velocity versus temperature for specific activation energies under the writing (applied field when ±5 V are applied) and reading (built-in field from the work function offsets with the contacts) conditions. These drift velocities are plotted in Fig. 4a, for the activation energies 0.5, 1.02, and 1.3 eV, as a function of temperature. The velocities described above that lead to an appropriate operational window are marked as the R-Line and the W-Line. It is obvious that there are no conditions where the velocities are appropriate both for a 10 year retention (solid lines must be below the R-Line) and a 100 ns writing time (dashed lines must be above the W-Line).

In other words, there is no combination of the three primary factors that control the timescale of device evolution that lead to a reasonable operational window for Schottky memristive devices based on uniform ionic motion to perform in memory applications. Figure 4a reinforces the earlier discussion that, for a 1.02 (and 1.3) eV activation energy, one can achieve a 10 year retention at room temperature, but vacancies cannot move fast enough at temperatures up to 1200 K to achieve a 100 ns programming time. For a 0.5 eV activation energy, vacancies move fast enough at 900 K for 100 ns programming, but the velocity is always too high for 10 year retention. The similar shapes of the three curves illustrate that no value of the activation energy will satisfy this demanding requirement.

Of course, while Fig. 4a considers a wide range of temperatures and activation energies, it only considers two electric fields (1 and 0.31 MV/cm), the difference of which causes the separation of the dashed and solid curves. The electric field has an exponential relationship to the velocity, see (10). The field can be increased by applying larger programming biases. However, considering the electrical breakdown characteristics of oxides [22], applying a field

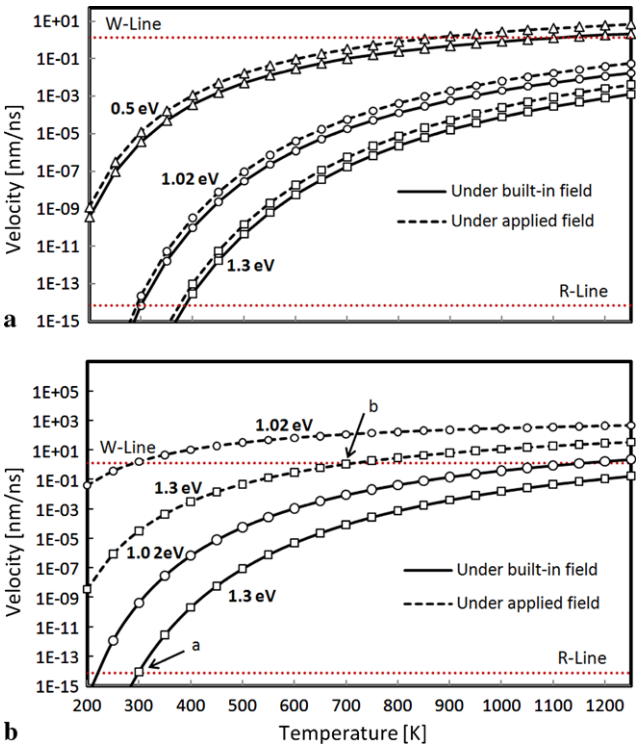

Fig. 4 (**a**) Vacancy velocity as a function of temperature under macroscopically observable electric field. Built-in field is 0.31 MV/cm (1.55 V/50 nm), and applied field is 1 MV/cm. The applied field is generated by applying 5 V bias over the 50 nm thick $SrTiO_3$ layer. (**b**) Vacancy velocity taking into account the local electric field, with $\chi = 300$ and $F = 0.2$ under the same biasing condition as part (**a**). In both plots R-Line indicates the maximum allowable velocity for 10 year retention and W-Line indicates the minimum required velocity for 100 ns programming

much larger than 1 MV/cm does not seem reasonable. For the 1.02 eV case, where the retention time is 10 years at room temperature, one would need to apply a field of ≈17 MV/cm at 1200 K for the writing time to be 100 ns, which seems extreme. Regardless of whether the region of ionic motion is uniform throughout the device or confined to a small portion of the device, the same tradeoffs among electric field, temperature and activation energy exist in all cases. Clear evidence that such memristive switches also fulfill all the technologically relevant device characteristics for memory application is lacking in the literature. Although throughout this work we have operated under the assumption of singly ionized vacancies, it has been suggested that vacancies in some cases may be doubly ionized [23]. To evaluate the impact of double ionization, simulations were carried out which indicated that when the same switching pulse (100 ns & ±5 V) is applied, the retention time for doubly ionized case was 6.35 µs compared to 1.58 µs for the singly ionized vacancies (with $E_a = 0.2$ eV). This difference is due to higher ON state and lower OFF state initial currents, which results from higher vacancy migration (thus, a stronger 'write' operation) due to stronger influence

of electric field on doubly ionized vacancies. Similar differences in retention time are observed for other values of activation energies as well. Although this increase is in the right direction, it does not lead to many orders of magnitude difference in time scale between switching and retention. Therefore, the fundamental dilemma remains the same regardless of the vacancy ionization level.

Two additional mechanisms have been posited that could lead to a wider operational window in memory technologies. One mechanism is that high currents lead to electromigration within the device (the ion motion is increased owing to a high number of electron impacts with the ion) [24]. This can be equated to an effective reduction in the activation energy [25]. In other words, we would need to compare the solid curve in Fig. 4a of one activation energy, say the 1.02 eV that has appropriate retention characteristics at room temperature (and low currents), to the dashed curve of another activation energy, say the 0.5 eV curve at 900 K that has the appropriate writing characteristics (in terms of speed). If electromigration is relevant to memristive switches then the current has to be capable (for activation energy of 1.02 eV) of decreasing the effective activation energy by a factor of 2 and increasing the temperature by a factor of 3 (900 K) as well. Although temperatures as high as 700–750 K have been reported in some switching devices [26, 27], typical reductions in activation energies during electromigration have been reported to be only ≈20% [25]. Therefore, it seems unlikely that an appropriate solution will be found by incorporating the electromigration effect.

Another mechanism that has been proposed is that the local electric field (acting on an atomic site) inside the dielectric is much greater than the macroscopically observed (applied) field [12]. According to the Lorentz relationship, the local field ξ_{local} at an atom in a dielectric is given by

$$\xi_{local} = \xi(1 + F\chi) \tag{11}$$

where χ is the dielectric susceptibility, and F is the Lorentz factor. Therefore, in materials with high dielectric susceptibilities exposed to large electric fields, such as $SrTiO_3$ where χ is ≈300, it is possible to achieve local fields that are significantly (orders of magnitude) higher than the external field, depending on the Lorentz factor, F. When the local field is large enough, the mobility (velocity) of vacancies is substantially increased since the field is in the exponential term of (5) and the barrier for ion hopping is related to the local field (Fig. 1). As a result, the difference in vacancy velocity under the built-in field and applied field significantly increases, as shown in Fig. 4b using $F = 0.2$ (though we did not include the field-dependent dielectric constant [22], which would complicate the picture somewhat).

The velocity determined using the local field during writing and reading, for specific activation energies (1.02 and 1.3 eV), are shown in Fig. 4b. It is apparent that the separation between the solid (low field) and dashed (high field) lines is much larger and the velocity is higher than that determined in Fig. 4a. In the case where the activation energy is 1.3 eV, Fig. 4b illustrates that the low field, low temperature retention time is greater than the value needed or 10 years (point a in Fig. 4b), while the local field increase combined with a reasonable temperature rise (700 K) leads to a 100 ns programming time (point b in Fig. 4b). In other words, by incorporating a local electric field value in a dielectric with a reasonable temperature increase from current flow, an appropriate operational window can be found quantitatively for memory technologies.

However, the appropriateness of inclusion of local field with regard to calculation of vacancy mobility remains to be verified. Several reports have described the effects of the local field (or field gradient) on ion displacements [28, 29] in dielectrics. It has also been argued that when ion hopping takes place between crystallographically similar sites, the local field plays no role in determining the hopping rate [30, 31]. From an energy conservation perspective, this argument certainly has merit. On average, the only electric field experienced by a migrating ion is the macroscopic field. Any local enhancement of that field in one part of the crystal must be balanced by reduction in other parts. While a physical parameter capable of causing static ion displacements was deemed worthy of consideration in our model, it is clear that experimental verification of such an effect is needed.

Along with the arguments presented above, there are several other complications also worth noting. The dielectric permittivity of thin film oxides can often be much lower than the bulk value [32], which would diminish this field enhancement. Also, the Lorentz factor can vary quite a bit among different locations in crystals [33, 34]. The quantitative improvement in device performance owing to a local field, if such an effect indeed exists, will be critically affected by such variations.

Simulation results presented here, incorporating only standard physical parameters, demonstrate quantitatively what values of electric field, temperature, and activation energy are required to achieve an operational memory device using uniform ion motion as the fundamental mechanism. While the results presented here were specific to a $SrTiO_3$ based Schottky type device, the model is general and can be applied to other device geometries and material systems. It quantitatively describes the fundamental conflict between retention and programming dynamics that is present in any resistance switching device based on homogeneous ion motion.

5 Conclusion

Using our model of uniform vacancy motion, we considered the effect of electric field, temperature, and activation energy on the switching and retention times of Schottky memristive devices. It is clear that no reasonable combination of those parameters lead to an appropriate operating window for memory devices. Secondary effects, such as electromigration, are not expected to significantly improve the switching time relative to the retention time. However, owing to the exponential dependence of vacancy mobility on electric fields present in the device, the inclusion of the local electric field on an ion site must be carefully examined as it would allow for engineering of viable devices.

Acknowledgements This work was supported in part by the Defense Advanced Research Projects Agency (DARPA) through the MISCIC Center at Carnegie Mellon under Grant HR0011-06-1-0047, in part by the Focus Center Research Program (FCRP)—Center on Functional Engineered Nano Architectonics, and in part by the Semiconductor Research Corporation under Contract Number 2006-VJ-1431.

References

1. D. Strukov, G. Snider, D. Stewart, S. Williams, Nature **431**, 80–83 (2008)
2. A. Sawa, Mater. Today **11**, 28–36 (2008)
3. J.J. Yang, J. Borghetti, D. Murphy, D.R. Stewart, R.S. Williams, Adv. Mater. **21**, 3754–3758 (2009)
4. K. Jung, J. Choi, Y. Kim, H. Im, S. Seo, R. Jung, D.C. Kim, J.S. Kim, B.H. Park, J.P. Hong, J. Appl. Phys. **103**, 034504 (2008)
5. J.J. Yang, M.D. Pickett, X. Li, D.A.A. Ohlberg, D.R. Stewart, R.S. Williams, Nat. Nanotechnol. **3**, 429–433 (2008)
6. C. Yoshida, K. Tsunoda, H. Noshiro, Y. Sugiyama, Appl. Phys. Lett. **91**, 223510 (2007)
7. S. Muraoka, K. Osano, Y. Kanzawa, S. Mitani, S. Fujii, K. Katayama, Y. Katoh, Z. Wei, T. Mikawa, K. Arita, Y. Kawashima, R. Azuma, K. Kawai, K. Shimakawa, A. Odagawa, T. Takagi, Tech. Dig., Int. Electron Devices Meet. 779–782 (2007)
8. R. Waser, R. Dittmann, G. Staikov, K. Szot, Adv. Mater. **21**, 2632–2663 (2009)
9. K. Szot, W. Speier, G. Bihlmayer, R. Waser, Nat. Mater. **5**, 312–320 (2006)
10. J. Blanc, D.L. Staebler, Phys. Rev. B **4**, 3548–3557 (1971)
11. D.B. Strukov, J.L. Borghetti, R.S. Williams, Small **5**, 1058–1063 (2009)
12. D.B. Strukov, R.S. Williams, Appl. Phys. A **94**, 515–519 (2009)
13. S.H. Jeon, B.H. Park, J.C. Lee, B.R. Lee, S.W. Han, Appl. Phys. Lett. **89**, 042904 (2006)
14. H. Shima, N. Zhong, H. Akinaga, Appl. Phys. Lett. **94**, 082905 (2009)
15. W. Jiang, D. Evans, J.A. Bain, M. Skowronski, P.A. Salvador, Appl. Phys. Lett. **96**, 092102 (2010)
16. R. Moos, W. Menesklou, K.H. Härdtl, Appl. Phys. A **61**, 389–395 (1995)
17. J. Maier, *Physical Chemistry of Ionic Materials* (Wiley, Chichester, 2004)
18. S.A. Chambers, Y. Liang, Z. Yu, R. Droopad, J. Ramdani, K. Eisenbeiser, Appl. Phys. Lett. **77**, 1662–1664 (2000)
19. G.M. Choi, H.L. Tuller, D. Goldschmidt, Phys. Rev. B **34**, 6972–6979 (1986)
20. R. Waser, T. Baiatu, K.-H. Härdtl, J. Am. Ceram. Soc. **73**, 1654–1662 (1990)
21. C.R. Crowell, V.V.L. Rideout, Solid-State Electron. **12**, 89–105 (1969)
22. H.-M. Christen, J. Mannhart, E.J. Williams, Ch. Gerber, Phys. Rev. B **49**, 12095–12104 (1994)
23. H. Yamada, G.R. Miller, J. Solid State Chem. **6**, 169–177 (1973)
24. K.G. Rajan, P. Parameswaran, J. Janaki, T.S. Radhakrishnan, J. Phys. D, Appl. Phys. **23**, 694–697 (1990)
25. H.B. Huntington, A.R. Grone, J. Phys. Chem. Solids **20**, 76–87 (1961)
26. U. Russo, D. Ielmini, C. Cagli, A.L. Lacaita, IEEE Trans. Electron Devices **56**, 193–200 (2009)
27. D.C. Kim, S. Seo, S.E. Ahn, D.-S. Suh, M.J. Lee, B.-H. Park, I.K. Yoo, I.G. Baek, H.-J. Kim, E.K. Yim, J.E. Lee, S.O. Park, H.S. Kim, U.-I. Chung, J.T. Moon, B.I. Ryu, Appl. Phys. Lett. **88**, 202102 (2006)
28. L.A. Errico, G. Fabricius, M. Rentería, P. de la Presa, M. Forker, Phys. Rev. Lett. **89**, 055503 (2002)
29. J.W. McPherson, J. Kim, A. Shanware, H. Mogul, J. Rodriguez, IEEE Trans. Electron Devices **50**(8), 1771–1778 (2003)
30. A.B. Lidiard, Handb. Phys. **20**, 246349 (1957)
31. R.W. Munn, J. Phys. C, Solid State Phys. **8**, 2721–2728 (1975)
32. C.T. Black, J.J. Welser, IEEE Trans. Electron Devices **46**(4), 776–780 (1999)
33. J.C. Slater, Phys. Rev. **78**, 748–761 (1950)
34. R.A. Parker, Phys. Rev. **124**, 1713–1719 (1961)